51st AIAA Aerospace Sciences Meeting including the New Horizons Forum and Aerospace Exposition
07 - 10 January 2013, Grapevine (Dallas/Ft. Worth Region), Texas

AIAA 2013-0375

Hypersonic Boundary-Layer Transition Experiments in the Boeing/AFOSR Mach-6 Quiet Tunnel

Andrew Abney*, Christopher Ward*, Dennis Berridge*, Roger Greenwood†,
and Steven P. Schneider‡
School of Aeronautics and Astronautics
Purdue University
West Lafayette, IN 47907-1282

Progress is reported for four of the experiments currently being conducted in the Boeing/AFOSR Mach-6 Quiet Tunnel (BAM6QT). Larger nozzle wall disturbances have been generated for use in the production of turbulent spots. The new design is currently undergoing refinement to produce more controlled disturbances. Two models were designed to maximize first mode instabilities in the BAM6QT. These models have been built and are currently being tested as a first step in developing a method for observing first mode instabilities in other hypersonic wind tunnels. The effect of discrete roughness elements on the stationary crossow instability was examined. Depending on the spacing of the roughness elements, the generation and breakdown of the stationary vortices was altered. A new 3-inch shock tube at Purdue has been tested and work on calibrating PCB-132 sensors has begun. Weak shocks with pressure rises less than 0.1 PSI have been created, and the PCB-132 sensors appear to have a linear response at small amplitudes, though results below 0.1 PSI are ambiguous.

Nomenclature

Re	Reynolds number	t	time
T	temperature	x	axial coordinate
Subscripts		*Abbreviations*	
0	stagnation condition	TSP	Temperature-Sensitive Paint
		SB	Schmidt-Boelter heat transfer gauge

I. Introduction

Hypersonic boundary-layer transition prediction is difficult due to high levels of uncertainty. The state of the boundary layer at hypersonic velocities can have a large impact on heat transfer rates, skin friction, and other boundary layer properties. Prediction of laminar to turbulent transition is difficult due to a lack of understanding of the fundamental processes which lead to transition, even in low noise environments.

Many transition experiments have been carried out in conventional ground-testing facilities over the past 50 years.[1] Unfortunately, the boundary layers studied were contaminated by noise radiated from the

*Research Assistant. Student Member, AIAA
†Research Assistant. Senior Member, AIAA
‡Professor. Associate Fellow, AIAA

turbulent boundary layer along the nozzle wall.[2] These noise levels, typically 1-3% of the mean pressure, are one to two orders of magnitude larger than those observed in flight.[3,4] These high noise levels can cause transition to occur much earlier than in flight.[2,3] In addition, the mechanisms of transition in small-disturbance environments can be changed or bypassed altogether in high-noise environments; these changes in the mechanisms can change the parametric trends in transition.[4] In order to improve transition prediction, mechanism-based methods must be developed, supported in part with measurements of the mechanisms in quiet wind tunnels.

A. The Boeing/AFOSR Mach-6 Quiet Tunel

The Boeing/AFOSR Mach-6 Quiet Tunnel (BAM6QT) is the largest operational hypersonic quiet tunnel in the world; the only other is the former NASA Langley Mach-6 Quiet Tunnel located at Texas A&M University. The BAM6QT is a Ludwieg tube design, consisting of a long driver tube section with a converging-diverging nozzle at the downstream end. A diagram of the tunnel is given in Figure 1. The driven section of the tunnel is separated from a vacuum tank by a set of two burst diaphragms. During operation, the tunnel is pressurized to the desired stagnation pressure, the downstream end is brought to vacuum, and the gap between the diaphragms is kept at half of the difference between the upstream and downstream sections. To begin a run the air between the diaphragms is evacuated and the diaphragms are burst, resulting in an expansion wave traveling upstream. The expansion wave reflects between the contraction section and the end of the driver tube. The stagnation pressure remains quasi-static throughout the run, dropping with each reflection cycle. This results in a quasi-static drop in Reynolds number throughout the run.

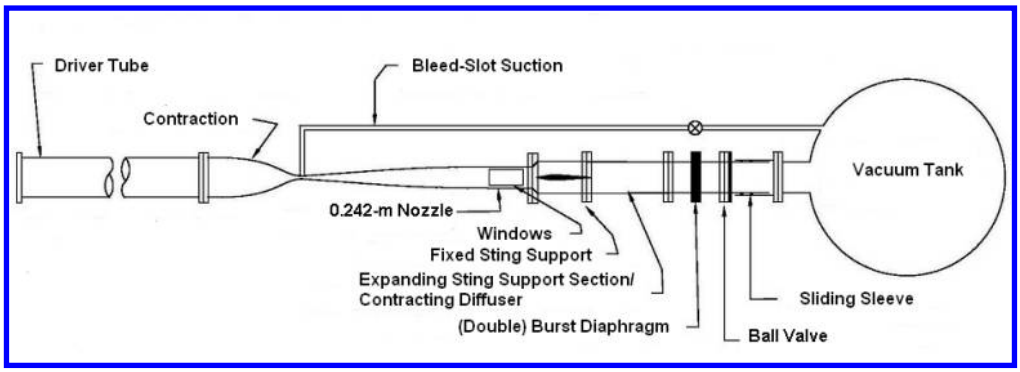

Figure 1. Schematic of the Boeing/AFOSR Mach-6 Quiet Tunnel

The BAM6QT is designed specifically to maintain a laminar boundary layer along the nozzle wall, resulting in noise levels on the order of 0.05% of the mean. This is achieved through several design features. The contour of the diverging section of the nozzle was lengthened to reduce the amplification of the Görtler instability. The throat and diverging section of the nozzle wall are polished to a mirror finish to reduce the probability of roughness induced transition, and the air supply is filtered to eliminate particulate larger than 0.01 micron. Lastly, just upstream of the throat is an annular bleed slot in the contraction. This slot removes the boundary layer that develops along the contraction wall, allowing a fresh laminar boundary layer to grow along the nozzle wall. The BAM6QT can also operate as a conventional tunnel by closing the valve that connects the bleed slots to the vacuum tank.

II. Towards improvement of turbulent spot generation on the nozzle wall of the BAM6QT

The process of boundary-layer transition can occur over significant portions of a hypersonic vehicle body.[5] The pressure fluctuations in this transitional region are higher in amplitude than those in a fully turbulent flow.[6] The passage of turbulent spots in the transitional region results in significant pressure fluctuations

which can vibrate internal components of vehicles. This is a result of the flowfield alternating between laminar flow and the passage of coherent structures in the turbulent spot. It is therefore essential that an accurate turbulent spot model of transition is developed for use in hypersonic vehicle design. Early studies of turbulent spot transition showed little interaction between merging spots[7] outside of the superposition of the merging spots area. However, recent DNS work by Sandham[8] has shown that the spanwise merging spots in supersonic boundary layers feature increased upwash in the lateral edges of the spots during coalescence. This results in an inflectional velocity profile in the merging wingtips, producing new coherent structures. Makita and Nishizawa[9] showed similar experimental results at low speeds. The pressure field underneath merging spots is still poorly understood.

Investigations conducted in the BAM6QT by Casper[10,11] used a pulsed-glow perturber to generate turbulent spots in the nozzle-wall boundary layer. The perturber produced second-mode-instability wave packets that broke down into turbulence as they convected downstream. Prior versions of the perturber consistently produced sparks along the nozzle wall, but any measurements taken were contaminated with high levels of electromagnetic interference (EMI). Occasionaly, the revised perturber design would still generate sparks superimposed upon the pulsed glow, but they were not repeatable and again produced large amounts of EMI. Any pulses contaminated with spark induced EMI were removed from the data set. Unfortunately, the pulsed glow perturbations did not show significant spanwise growth until they transitioned to a turbulent spot, which occurred a significant distance downstream of the perturber. This result made the measurement of lateral merging of turbulent spots impossible within the given measurement limits of the BAM6QT nozzle wall. It is therefore necessary to improve the production of turbulent spots along the BAM6QT nozzle wall to enable the measurement of the pressure fluctuation field underneath laterally merging turbulent spots.

Two methods are currently under investigation to produce stronger perturbations in the BAM6QT nozzle-wall boundary layer. The first method is an improvement upon the existing pulsed glow perturber in use at Purdue. Casper discovered that the glow perturbations created by the existing hardware lasted approximately 200 μs.[10] In order to reduce the length of the perturbations, a Belkhe HTS 121-01-HB-C high voltage push pull switch (HVT) was ordered. This switch replaces the timing circuit and ignition coil of the previous design. A 10-kV DC power supply will be used to power the circuit. The HVT will allow for controlled perturbations to be generated with pulse durations as short as 70 ns. The lower bound of the perturbation length as built will be determined by the final capacitance of the wired circuit. The Belkhe switch is scheduled to arrive by January 2013, and testing of the new design will begin at that time.

The second perturber under investigation is a pulsed jet perturber. A Parker 009-1669-900 pulse valve, commonly used as a molecular beam source in Time of Flight Mass Spectroscopy,[12] is used to inject a jet of air into the nozzle wall boundary layer during a run. The valve is connected to a nozzle-wall insert, which has a 1 mm orifice for the flow to pass through to the nozzle wall. When operated, the pressurized air behind the valve expands into a supersonic jet in the low static pressure present during tunnel operation. This valve is operated by a driver designed in house at Purdue's Jonathan Amy Facility for Chemical Instrumentation, which reduces the response time of the valve by powering the solenoid coil with a 300 V pulse. This pulse can be set anywhere from 40–300 μs. If additional open time is needed, a holding voltage of approximately 8 V is used to keep the valve open, currently limited to a minimum of 120 μs total valve open time by the driver hardware.

Sensor #	Distance Downstream of Perturber [m]
1	0.277
2	0.378
3	0.454
4	0.704
5	0.857
6	0.908

Table 1. Pressure transducer locations relative to perturber.

Numerous tunnel runs were conducted in an attempt to optimize valve operation. Valve performance was measured through the use of 6 Kulite XCQ-062-15A pressure transducers arranged in a streamwise array along the nozzle wall centerline at locations given in Table 1. Initially the valve performed inconsistently resulting in little useful data. This was a result of the poor wear characteristics of the stock polytetrafluoroethylene (PTFE) poppets. Due to the poor wear resistance, the sealing face of the PTFE poppet deformed, and countersunk completely within the orifice, preventing the orifice from opening under travel. Once this was realized, higher strength polyether ether ketone (PEEK) poppets were ordered to improve the wear characteristics of the valve. Figure 2 shows the difference in wear experienced by the two materials over a similar usage cycle of approximately 20 tunnel runs.

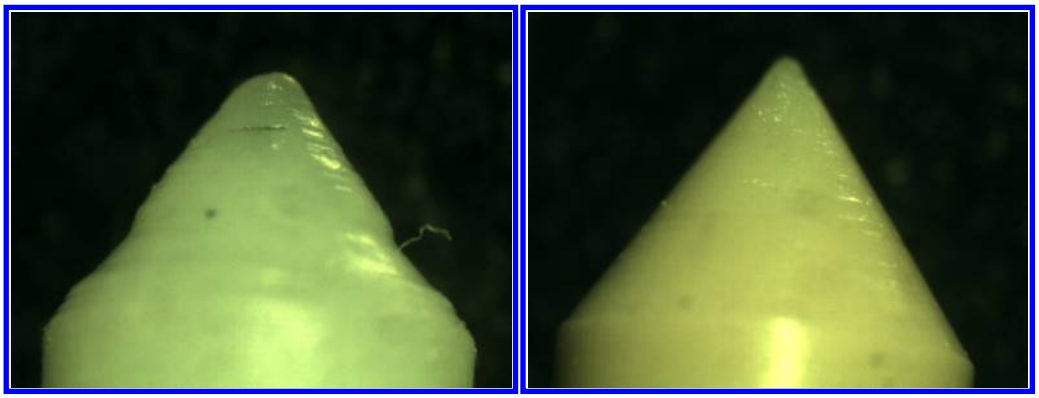

(a) PTFE poppet (b) PEEK poppet

Figure 2. Wear of two poppets of different materials after approximately 20 tunnel runs

Once the PEEK poppets were installed, the perturber system consistently produced patches of turbulence in the nozzle wall boundary layer. Figure 3 shows the ensemble average of 25 perturbations over a 0.5-second portion of the run as the disturbance moves down stream at a unit Reynolds number of 12.0×10^6/m, as well as a single sample. Ensemble averaging tends to reduce turbulent peaks. At present, the pulses last approximately 800 μs at the first measurement position. It seems that transition to turbulence occurs prior to this location. The legend in the plot indicates the distance downstream of the perturber, and each pressure trace is offset relative to the transducer position downstream. As the perturbation convects downstream, it appears that packets of second mode waves trail the turbulent patches.

Thus, large perturbations in the BAM6QT nozzle-wall boundary layer have been obtained, but currently the duration is longer than desired. It is uncertain at this point whether the perturber is producing true turbulent spots or a quasi steady-state flowfield. In order to reduce the duration of the perturbation two methods are being used. A new modified valve driver is under construction which will provide the ability to eliminate the low voltage pulse entirely, thus reducing the total valve-open time. Secondly, the poppets have been modified to add a cylindrical face on the sealing surface. It is hoped that this face will countersink the poppet into the exhaust orifice, and reduce the valve-open time to a small fraction of the time for a stock valve. This modification can be seen in Fig. 4.

III. Crossflow Instability and Transition on a Cone at Angle of Attack

There are several instabilities that can cause transition in a three-dimensional boundary layer, including the centrifugal, streamwise, and crossflow instabilities. For an axisymmetric cone in hypersonic flow pitched at an angle of attack, a circumferential pressure gradient is created due to a stronger shock near the windward ray compared to the leeward ray. The circumferential pressure gradient causes the inviscid streamlines to be curved. In the boundary layer, there is an imbalance between the pressure gradient and the centripetal acceleration because the streamwise velocity is reduced, but the pressure gradient does not change. This imbalance causes a secondary flow (crossflow) in the boundary layer perpendicular to the inviscid streamlines.

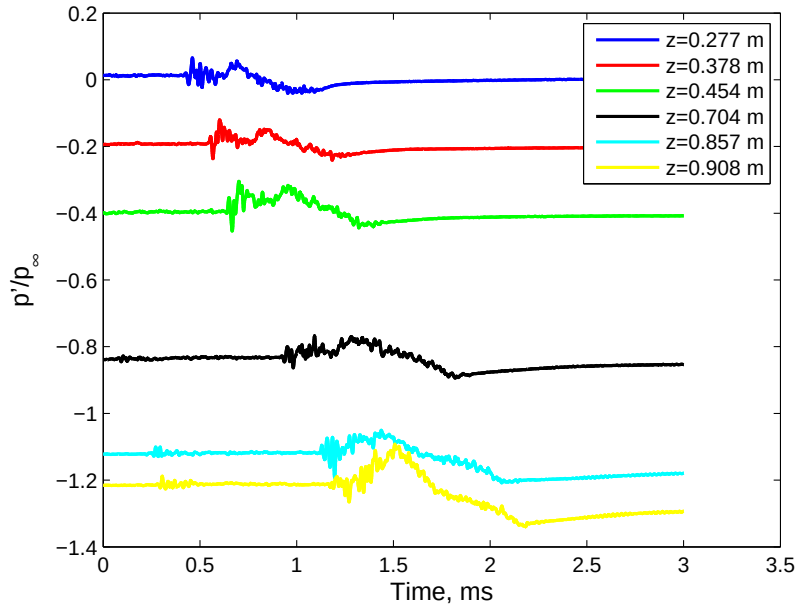

(a) Ensemble Average of 25 Samples

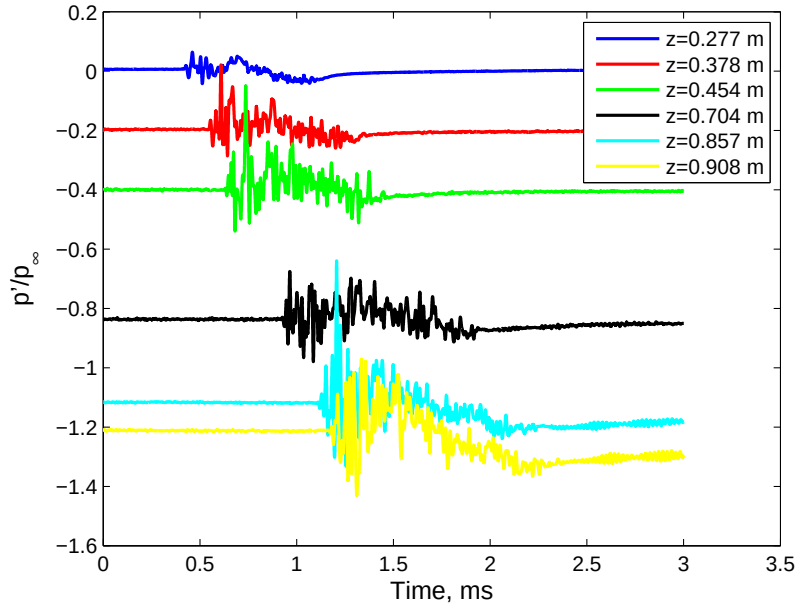

(b) Sample Disturbance

Figure 3. Turbulent Patches generated by Pulsed Air purturber. Re = 12.0×10^6/m, p_0 = 160.7 psia

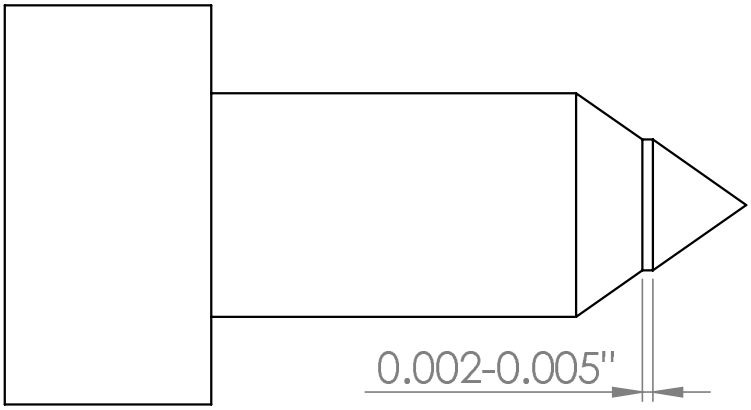

Figure 4. Schematic of modified PEEK poppet for reducing total valve-open time

Crossflow must vanish at the wall and the edge of the boundary layer, creating an inflection point in the crossflow velocity profile.[13] Crossflow is thus inviscidly unstable. The instability manifests as co-rotating vortices forming around the inflection point. Crossflow waves can be either travelling or stationary with respect to the surface. It has been verified experimentally for low speeds that the stationary waves tend to dominate in low-disturbance environments such as in flight or in low-noise tunnels, while the travelling waves tend to dominate in high-disturbance environments such as conventional tunnels.[14]

The stationary waves appear to be sensitive to small roughness placed near the waves neutral point. Saric has had much success in using discrete roughness elements on a swept wing at low speeds to control the stationary vortices.[13,15] Depending on the spacing of the roughness, Saric was able to force certain wavelengths of the stationary vortices, and was able to delay transition.

Corke et al. were able to control the stationary vortices on a cone at angle of attack with small roughness elements placed near the nosetip at Mach 3.5.[16,17] By forcing stationary wavenumbers greater than the most naturally amplified wavenumber, transition was delayed. The author's present research will look at attempting to control the stationary vortices at Mach 6 using discrete roughness elements.

A. Results

1. Roughness Results

Tests were performed in November 2012 to obtain global heat transfer from the temperature-sensitive paint on a 7° half-angle cone at 6° angle of attack. TSP is calibrated to heat transfer using the method discussed in Reference 18. Discrete roughness elements were placed around the azimuth, 50.8 mm (2 inches) axially from the nosetip. This axial location is near the neutral point of the most unstable stationary modes according to computations by Li et al.[19] These computations state that the most naturally amplified stationary modes have wavenumbers between 45 and 55. The discrete roughness elements, or dimples, were created by pressing a conical stainless steel rod into a torlon section of the cone. This is a similar method to the one used by Schuele.[17] The torlon section extended axially from 38.1–50.8 mm (1.5–2.5 inches) from the nosetip. Three different torlon sections were manufactured. One with no dimples, one with 50 dimples (spaced 7.2° apart), and one with 72 dimples (spaced 5° apart). The 50-dimple case should, theoretically, force the most unstable stationary crossflow wavenumber. The 72-dimple case should force a wavenumber greater than the most unstable wavenumber. Saric[15] and Corke[16] found that forcing a wavenumber greater than the most unstable wavenumber suppressed the most unstable modes, and crossflow-induced transition was delayed. The following tests will begin to examine if this same effect can be seen at Mach 6.

Saric et al.[20] suggest that the diameter of the roughness elements divided by the wavelength of the desired wavenumber should be greater than 0.5 for effective forcing. It is not known if this ratio should be

altered for hypersonic speeds. It was decided to create dimples with a diameter to wavelength ratio of 0.55. For the 50-dimple case, the dimple diameter and depth are nominally 400 and 280 μm. For the 72-dimple case, the dimple diameter and depth are nominally 250 and 180 μm. These diameters and depths are not the true values, since complete plastic deformation of the torlon did not occur.

A Mitutoyo Surftest SJ-301 surface roughness profilometer was used to measure the profile of the dimples. The 72-dimple case created dimples too small for the profilometer to measure. More sophisticated techniques will be needed to measure the smaller dimples. Figure 5 shows the profile of a dimple created for the 50-dimple case. A smooth case was added for reference. The depth was measured as approximately 40 μm, smaller than the expected value of 280 μm. When the stainless-steel rod was pressed into the torlon, some material was pushed out, creating the peaks in the profile. This created a larger effective depth of the dimple, approximately 70 μm. The effective diameter of the dimple is 300 μm. It could also be said that the dimple has an effective diameter of approximately 600 μm, based on where the profile departs and returns to the smooth case. There is some uncertainty in the measurements since it is not known if the profilometer traversed the middle of the dot, and therefore the depth and diameter may be incorrect. The drill press used to push the conical rod into the torlon had an approximately 20-μm uncertaintty in depth. A Newmark RT-5DR Manual Rotary Stage was used to determine azimuthal placement of each dimple, and has a quoted accuracy of 0.00225° . Larger dimples were created on a test piece of torlon with a diameter of approximately 1000 μm. The diameter and the depth of the dimples were uniform within 5%. It is difficult to determine the uniformity of the dimples used in the experiments due to the errors associated with the current measuring technique. The most important aspect of the dimple for effective forcing is not known at hypersonic speeds. It may be the protruding surface height, the cavity depth or the dimple diameter.

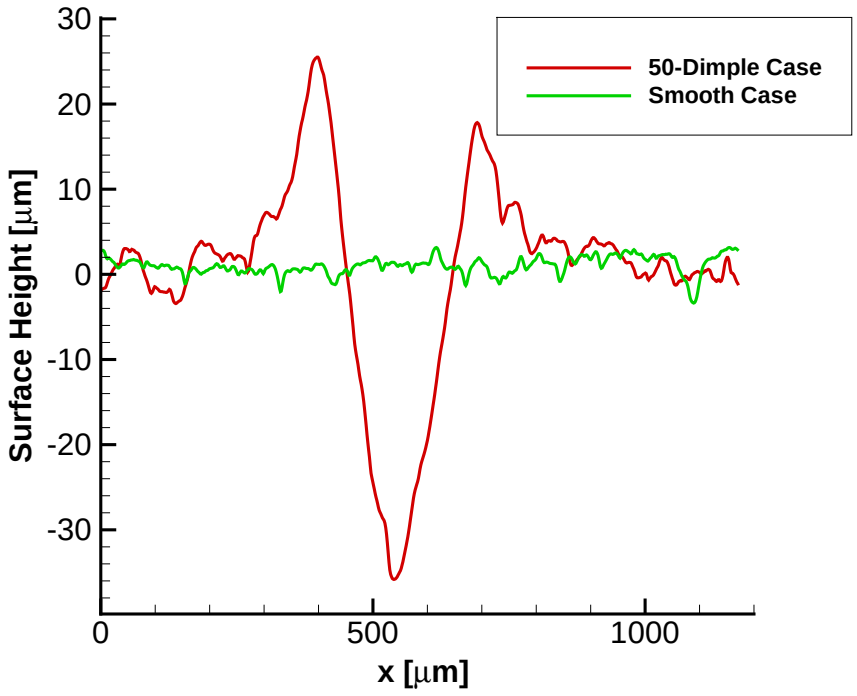

Figure 5. Profile of discrete roughness element (dimple).

The first set of tests were done at a unit Reynolds number of 10.5×10^6/m. TSP images with global heat transfer are shown in Fig. 6, with 0, 50 and 72 dots around the azimuth, 2 inches from the nosetip.

The smooth case clearly shows the stationary vortices. Transition appears to be occurring near the lee ray, but possibly only on the upper half of the cone. The smooth-case results qualitatively agrees with previous measurements by the author,[21] although the exact spacing of the stationary vortices may be different. The stationary vortices in the smooth case are likely generated by small irregularities in the machined or painted finish of the cone, which is not necessarily the same from one set of tests to the next. When 50 dimples are added, transition appears to occur further upstream, and the vortices break down on both the lower and upper half the of the cone. The stationary vortices appear to be more symmetric about the leeward ray, as compared to the smooth case. Theoretically, a regular pattern of dimples is now generating the stationary vortices, rather than a random distribution of small roughness as in the smooth case. Therefore, a more symmetric generation of stationary vortices would be expected. The data to determine if the dimples are creating a wavenumber of 50 and if the vortices are body-fixed are still being collected and processed.

The 72-dimple case also shows transition near the lee ray, but qualitatively appears to be delayed or less widespread than the 50-dimple case. This would agree with the previously mentioned computations by Li et al.[19] A wavenumber of 72 should be more stable and transition further downstream than a wavenumber of 50, while suppressing the most unstable stationary modes with wavenumbers near 45–55.

Spanwise heat transfer profiles at an axial distance of 0.35 m for the three TSP images in Fig. 6 are shown in Fig. 7. It is clear each set of dimples is creating a different pattern of stationary vortices on the bottom half of the cone (positive spanwise reference values), but interestingly the vortex pattern for all three cases seems similar near -0.02 m. The 50-dimple case is also creating larger amplitude vortices, especially near -0.01 m and 0.02 m. The broader peaks at these spanwise locations also suggest that the 50 dimples are inducing breakdown of the stationary vortices earlier than the other two cases.

Plotted in Fig. 8 are spanwise heat transfer profiles further downstream, at 0.38 m. All three profiles show larger heat transfer on the upper half of the cone (negative spanwise reference values) compared to the 0.35 m profiles suggesting that the vortices are beginning to break down. There are fewer large and distinct peaks in the 50-dimple case. This implies that the transition process is further along for the 50-dimple case, compared to the other two cases.

2. Repeatability Tests

It is important to determine if the results found are repeatable. Each case (0, 50 and 72 dimples) was tested twice at approximately the same Reynolds number. For the smooth case, these two tests were performed back-to-back without opening the tunnel. For the 50 and 72 dimple case, the tunnel was opened, the torlon section was removed and reinstalled, and the repeat test was performed immediately after.

Figure 9 shows spanwise heat transfer or temperature profiles at an axial location of 0.35 m. For the smooth case, the two profiles are very similar. Note that for the 50-dimple case, the Schmidt-Boelter heat transfer gauge did not work for the repeat run, therefore the temperature is plotted instead of heat transfer. The peaks and the valleys in the 50-dimple case profile appear to line up quite well. The repeat run shows higher overall temperatures, but this is likely due to the lower wall temperature, or slightly different tunnel conditions. Finally, the 72-dimple case shows decent repeatability. The slight differences in heat transfer once again are likely due to a different wall temperature, or slightly differing tunnel conditions. At 0.02 m, there is an additional peak in the repeat case. It is not known why this peak does not appear in the original run. Overall, the three cases appear to create fairly repeatable results

IV. First-Mode Dominant Design and Initial Results in the Boeing-AFOSR Mach 6 Quiet Tunnel

The objective was to design and build a slender model with significant first-mode instability waves that can be easily measured in the BAM6QT. This would serve as a stepping stone to developing a method for observing first-mode instabilities on blunt models. This method could then be refined and used in other hypersonic wind tunnels. A systematic approach culminating in the use of a hypersonic computational package was used in this design process.

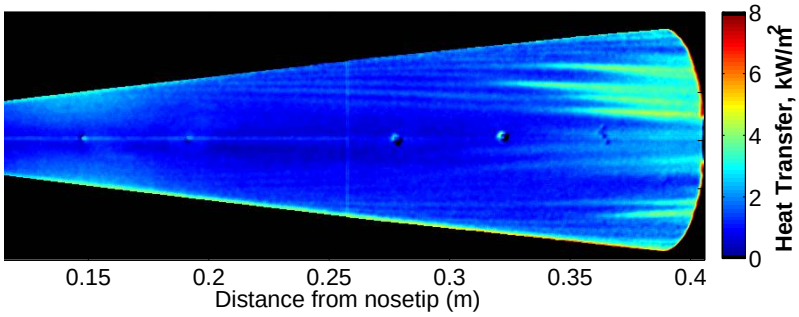

(a) Smooth. T_{wall} = 297.6 K.

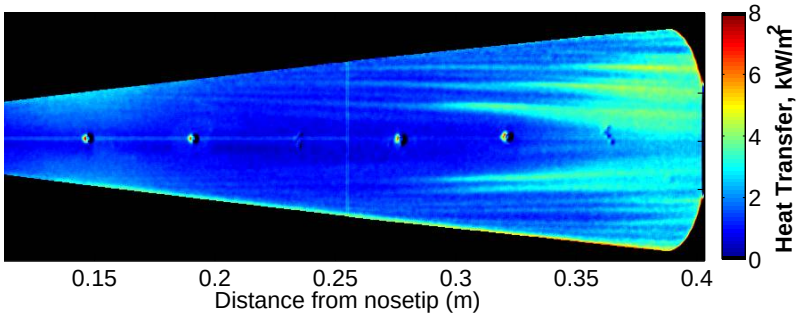

(b) 50 dots. T_{wall} = 295.3 K.

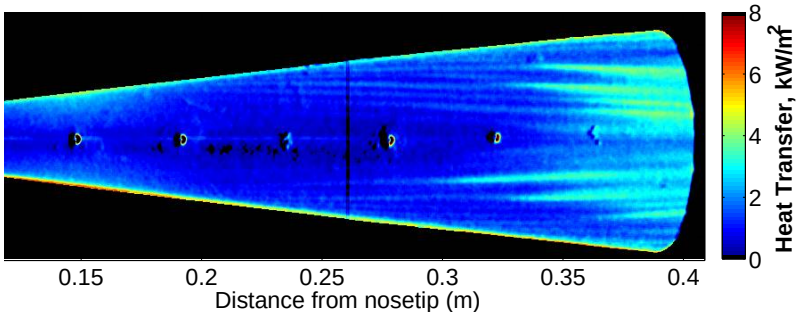

(c) 72 dots. T_{wall} = 299.7 K.

Figure 6. TSP images of 7° half-angle cone at 6° angle of attack. Lee side of the cone. Quiet flow. Re = 10.5×10^6/m. p_0 = 149 psia. T_0 = 426 K.

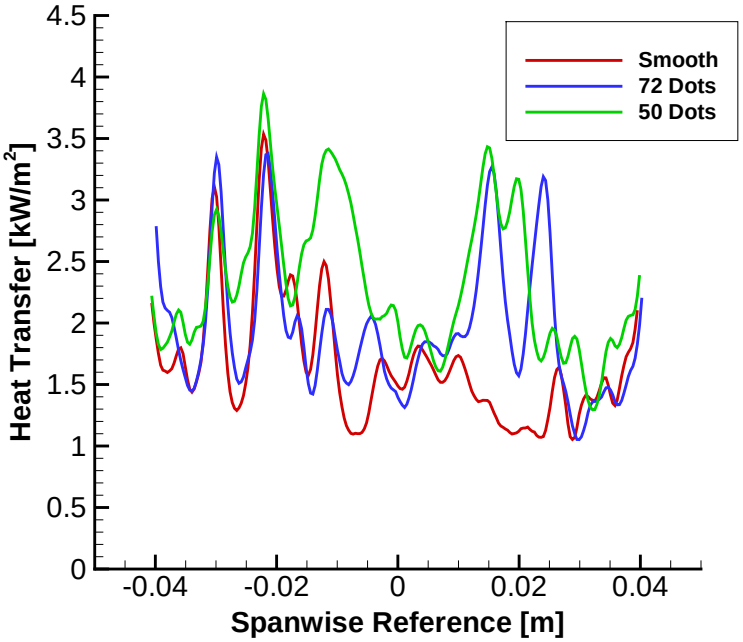

Figure 7. Spanwise temperature profiles at an axial distance of 0.35 m from the TSP images in Fig. 6. Re = 10.5×10^6/m. p_0 = 149 psia. T_0 = 426 K.

The Stability and Transition Analysis for Hypersonic Boundary Layers (STABL) software suite[22] was used at Purdue University to calculate the mean flow and stability characteristics of a series of geometric configurations in an effort to find the design that would provide the best opportunity to measure first-mode instability waves in the BAM6QT. The design process brought to light many characteristics of first and second-mode instability wave growth and resulted in a cone-ogive-cylinder design that is currently being tested.

A. Introduction

Significant progress has been made in the measurement of second mode instability waves on sharp cones using high frequency sensors. This process has been used successfully in several different hypersonic wind tunnels[23] with the end goal of determining what factors affect second mode transition on a given geometry. We desire a comparable method of detecting first-mode instability waves with pressure sensors. Initial work in the BAM6QT would develop techniques that can be applied in many different hypersonic tunnels. These verified techniques could then be used to measure possible first-mode waves on other geometries of interest, such as blunt geometries of interest to NASA, cowl inlets on scramjet vehicles, and other geometries of interest to the Department of Defense.[24]

B. Desired Geometry and Constraints

The basic geometry was developed by the interactions of several individuals.[24] The idea was to find the simplest axisymmetric geometry that maximized the first-mode instability waves in order to induce transition. In order to ensure that transition was induced by the first-mode instabilities, it was also necessary to ensure that the amplitudes of any other instabilities were significantly less than the first mode. An axisymmetric design was necessary to simplify both the computational analysis and the machining of the physical model.

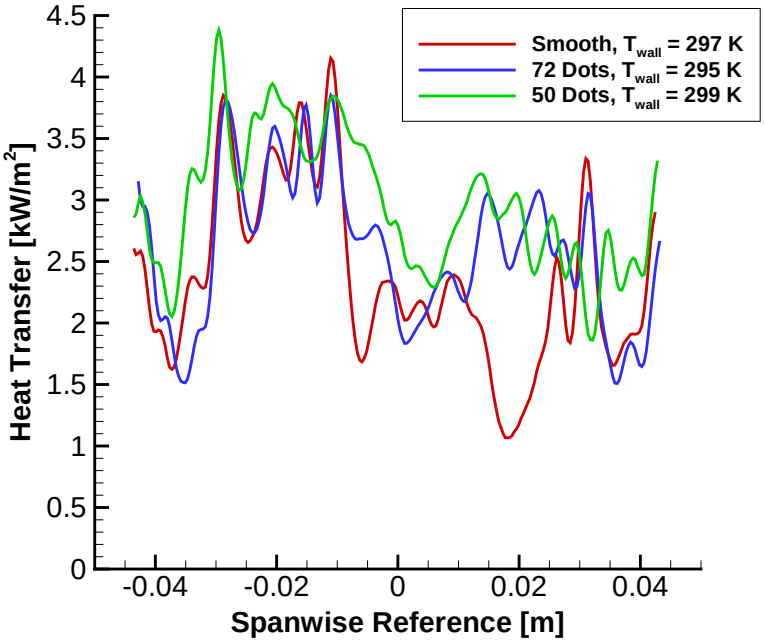

Figure 8. Spanwise heat transfer profiles at an axial distance of 0.38 m from the TSP images in Figure 6. Re = 10.5×10^6/m. p_0 = 149 psia. T_0 = 426 K.

The simplest design would be a sharp cone, but preliminary calculations by Meelan Choudhari[25] indicated that the vertex angle would become too large for a simple cone geometry to start in the BAM6QT while still providing the necessary length to obtain large waves.

The next design consideration was to use a more complex shape. It would begin with a sharp cone nosetip to lower the edge Mach number sufficiently for first-mode instabilities to dominate. At a certain diameter, this cone would merge into an ogive-cylinder of a constant diameter that would allow adequate length for the first-mode instabilities to grow large enough to induce transition on the model. If this design proved to be insufficient to induce transition within a reasonable length, a slight flare could be added to the cylinder that would maintain the boundary layer at a fairly constant thickness. This would allow the same frequency instability waves to amplify over a longer distance and increase the possibility of transition within a reasonable distance downstream. This same concept has been used successfully to induce very large second mode waves in the BAM6QT[21] on a very sharp flared cone.

C. Computational Setup

The design process included several steps of increasing complexity and fidelity. An external flow method of characteristics code developed by Zucrow and Hoffman[26] was used initially to determine a feasible geometry with an edge Mach number ≤ 5 where first-mode instabilities tend to dominate. Once a general design space was determined, further analysis was conducted using a hypersonic flow and stability analysis code (STABL) developed at the University of Minnesota.[22]

Multiple geometries were run in STABL. Initially, two design parameters were used to describe the geometry while all the other parameters were held constant. The independent parameters chosen were the leading edge cone half angle and the diameter of the cylinder. An example of one of these geometries is shown in Fig 10.

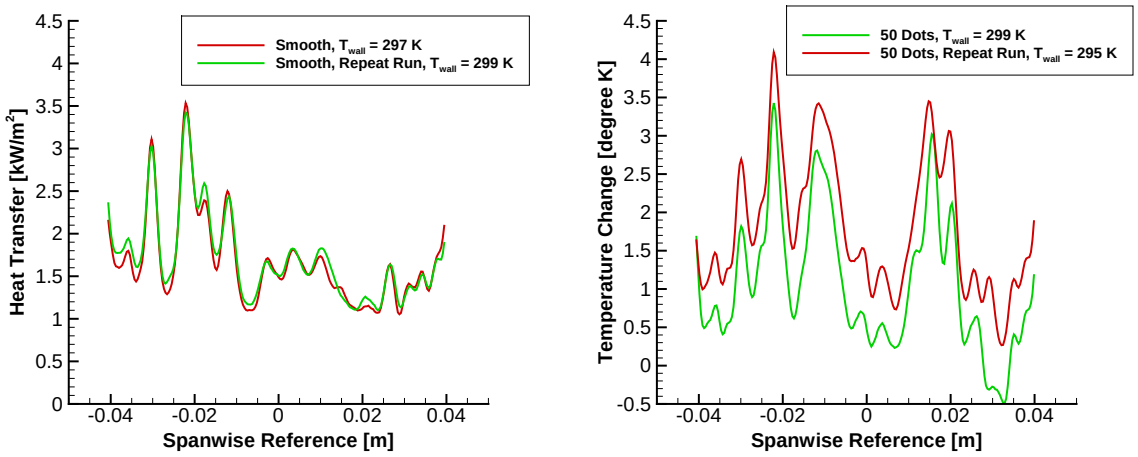

(a) Smooth. T_{wall} = 297.6 K.

(b) 50 dots. T_{wall} = 295.3 K.

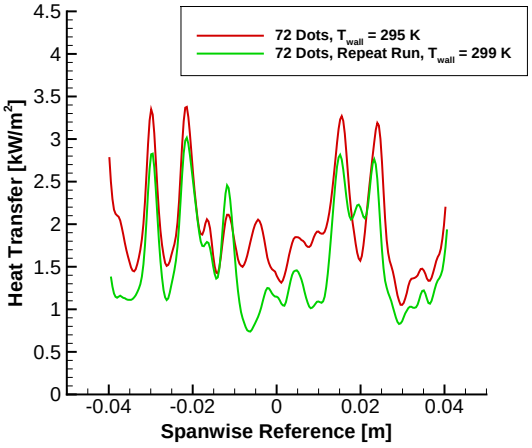

(c) 72 dots. T_{wall} = 299.7 K.

Figure 9. Spanwise heat transfer and temperature profiles at an axial distance of 0.35 m. Re = 10.5×10^6/m. p_0 = 149 psia. T_0 = 426 K.

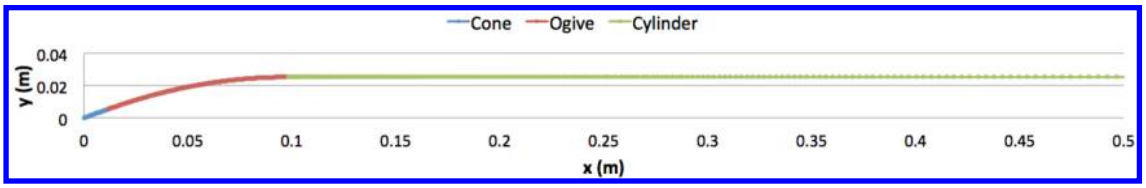

Figure 10. Cone-Ogive-Cylinder geometry with 25 degree leading edge half angle and 5 cm diameter.

Each case was run under conditions that simulate the BAM6QT at a stagnation pressure of 160 psia. Upon selecting an optimal design with these two parameters, their optimized values were set constant and a flare was added to the model downstream of the ogive.

D. Computational Results

1. Impact of Leading Edge Cone Angle

The leading edge cone angle had the greatest impact on the edge Mach number which in turn dictated whether the first or second mode instability was dominant. It was estimated that the first mode instabilities would start to become more dominant when the edge Mach number decreased to about Mach 5. Fig 11 shows the variation of edge Mach number due to the leading edge cone angle for various half cone angles on a cone-ogive-cylinder with a diameter of 5 cm.

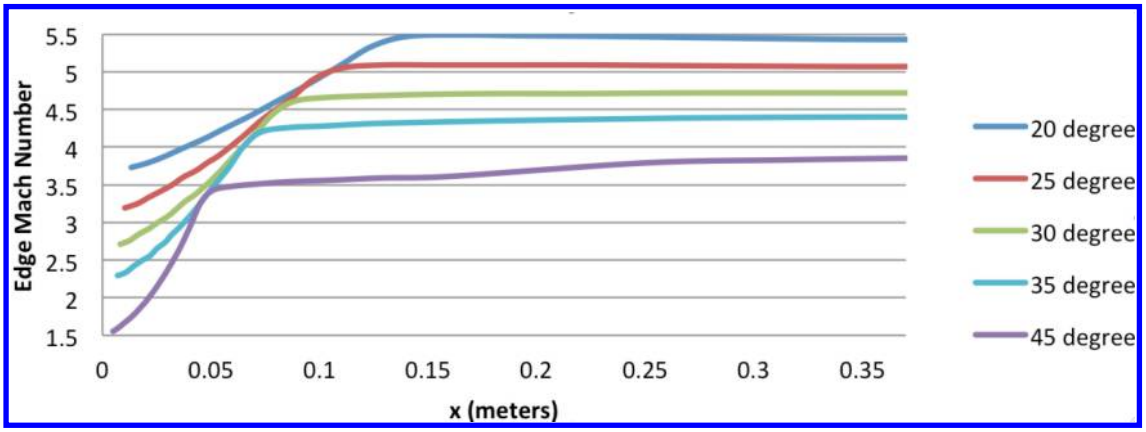

Figure 11. Edge Mach Number values for Cone-Ogive-Cylinder geometries with varying Leading Edge Half Cone Angles.

The numerical calculations showed that at the trailing end of a cone-ogive-cylinder with a leading cone half angle of 25 degrees, the first and second mode instabilities were approximately equal. As shown in Table 2, at cone half angles less than 25 degrees, the second mode instability became dominant and at higher angles the first-mode N-factors were slightly larger than the 2nd mode N-factors. At even higher cone angles, the calculations showed a significant decrease in both first and second mode instabilities. However, all the instabilities are fairly weak.

2. Impact of Cylinder Diameter

Cylinder diameter had very little effect on the instabilities computed in STABL. Computations showed that as the cylinder diameter was increased from 5.1 to 7.6 centimeters (2 to 3 inches), the magnitude of the dominant N-factors remained fairly constant. However, the frequency of the instabilities decreased slightly as the diameter increased.

Table 2. Computed N-factors at 0.38m for first and second mode instabilities for various leading edge cone angles.

Leading Edge Cone Half Angle (degrees)	1st Mode N-Factor	2nd Mode N-Factor
20	0.05	3
25	2.1	1.8
30	1.9	1.3
35	1.6	0.7
45	0.7	0.3

3. Impact of Flare on Cylinder

Flare was added to the cylinder in order to maintain an approximately constant boundary layer thickness. This would allow the same frequency waves to be amplified over a longer distance and thus achieve larger N-factors on the model. A comparison of the flared and non-flared geometries is shown in Fig 12.

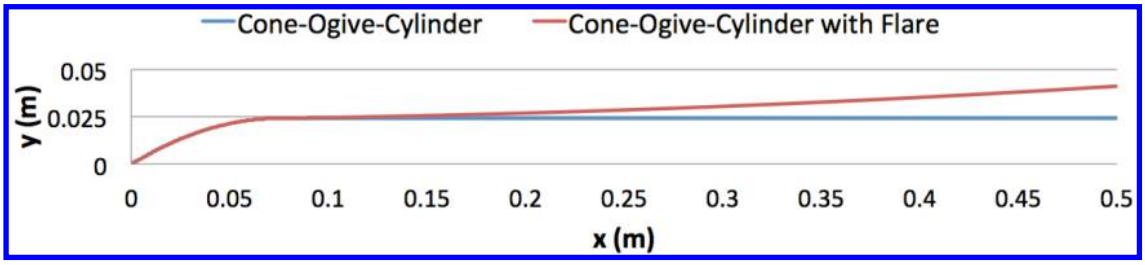

Figure 12. Comparison of cone-ogive-cylinder geometries with and without flare.

An unanticipated result is that the flare caused the second mode N-factors to increase at a much greater rate than for the first-mode waves. Because of this, the flared design had higher second mode N-factors at the trailing edge than first mode, even though in the original (non-flared) design the first-mode N-factors were larger.

Figure 13 on the following page shows the impact of the flare on the N-factors of the cone-ogive-cylinder with the 30 degree leading edge half angle. The flared and non-flared geometries are shown in Fig 12. Figure 13(a) shows the most amplified first mode instability on the cone-ogive-cylinder. Figure 13(b) shows the most amplified first mode instabilities on the flared cone-ogive-cylinder. They show that the frequency of the most amplified instability increases with the flare. The maximum N-factor also increases slightly.

In the same way, Figs 13(c) and 13(d) show the impact of flare on the second mode instabilities. The frequency of the most amplified instabilities increases due to the thinner boundary layer in the flared design. At the same time, the boundary layer stays at a near constant thickness allowing the same second mode frequencies to grow over a greater distance. The result is significantly higher second mode N-factors at the trailing edge of the flared geometry.

The reason the flare has a much greater impact on the second mode than the first mode is not completely understood. One possible explanation is that the second mode instabilities have a larger growth rate than the first mode but a more narrow band of frequencies over which they are amplified. That being the case, the constant boundary layer thickness of the flared design would allow the amplified second mode instability to grow over a greater distance and achieve higher N-factors. However, if the first mode instability has a wider band of amplified frequencies, it would grow more slowly than the second mode but over a greater distance on the non-flared design, resulting in greater N-factors at the trailing edge. This point is to be addressed more in the future.

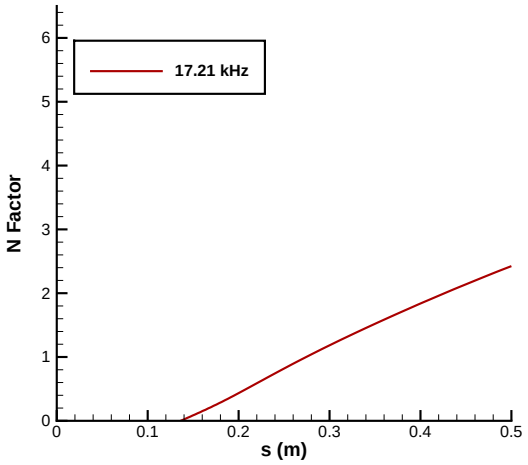

(a) Maximum First Mode N-factors on a Cone-Ogive-Cylinder.

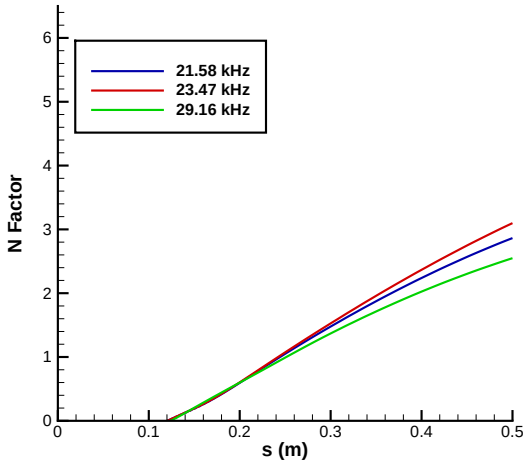

(b) Maximum First Mode N-factors on a Cone-Ogive-Cylinder with Flare.

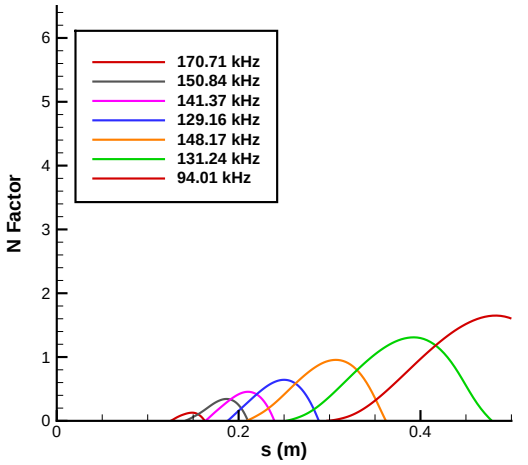

(c) Maximum Second Mode N-factors on a Cone-Ogive-Cylinder.

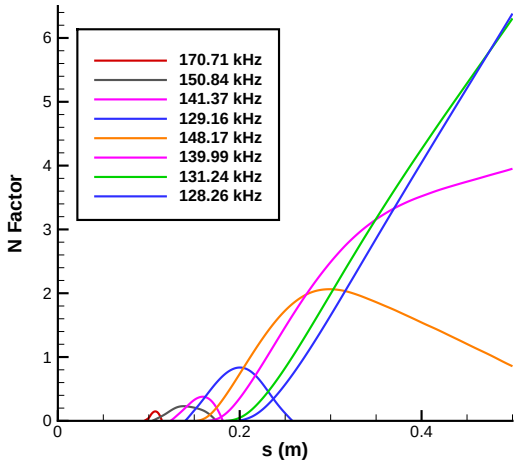

(d) Maximum Second Mode N-factors on a Cone-Ogive-Cylinder with Flare.

Figure 13. Plots showing the impact of flare on first and second mode instabilities.

4. *Cone-Ogive-Cylinder Design*

Because of the significant increase in the N-factors of second mode instabilities when the flare is added, flare was not used in the final design selected at Purdue. The final geometry was an axisymmetric cone-ogive-cylinder with a 30 degree leading edge half angle and a 1.9 inch diameter. The front half of the model is shown in Fig 12. Then, to allow the first mode instabilities to grow as long as possible the model was extended to a length of 1 meter [40 in]. One limiting factor of this long of a design in the BAM6QT is the shock from the leading edge of the model that reflects off the tunnel walls to impact the model further down in the test section. An exact location for this impact was not known during the design process.

5. *Flared Design*

In coordination with the Purdue design effort, an optimization tool was employed by Lindsay Kirk to maximize first mode instabilities. The optimized design was significantly different because the optimization did not stipulate that second mode instabilities be smaller than the first mode. This design was a very sharp cone with a slight flare down the length, reaching a diameter of 0.08 meters at 1 meter downstream. A curve fit was made to match the optimized design coordinates in order create the computational and experimental flared cone models. The curve fit is shown in Equation 1 and the design is plotted up to 0.75 meters in Fig 14.

$$y = 0.375x + 0.000115x^2 - 0.000001x^3 \tag{1}$$

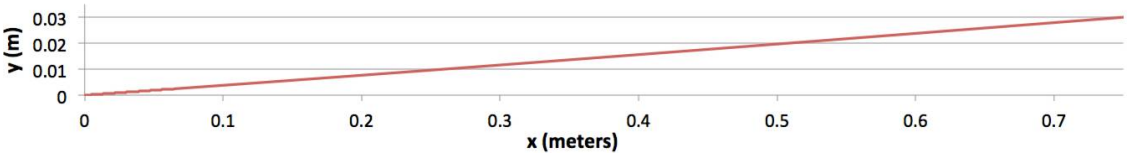

Figure 14. Flared Cone designed by Lindsay Kirk to optimize First Mode Instabilities.

A computational analysis of this design showed the first-mode N-factors over twice the magnitude of the Purdue design with a first mode N-factor at about 5 and a second mode N-factor of about 8.5 at 0.5 meters.

E. Experimental Results

Both of these designs were constructed in the Purdue machine shop. The nosetips were made out of stainless steel and the afterbody was made out of T6061 aluminum. Initial testing has begun at Purdue's BAM6QT. Kulite high frequency pressure transducers are starting to be used to try and capture the first-mode instabilities and Temperature Sensitive Paint is being used to identify flow features that may impact the instability waves.

1. *Cone-Ogive-Cylinder Results*

Due to the length of the Purdue design, it was believed that the reflected shock from the test section wall would impinge upon the model at some point. Because of the uncertainty of the location of this reflected shock and the impact it may have on the instabilities, the model was painted with temperature-sensitive paint and tested in the BAM6QT under a wide range of both noisy and quiet flow conditions. A picture of the completed cone-ogive-cylinder is shown in Fig 15 and Fig 16 is a picture of the model after the rear two-thirds was painted with TSP.

It was found that under noisy flow, the reflected shock impinged upon the model between about 0.66 and 0.68 meters from the leading edge of the model. The TSP result for the noisy flow shock is shown in Fig 17(a). Under quiet flow conditions, the shock is much more difficult to identify but it seems to impinge at a distance of about 0.85 meters from the leading edge. The TSP results are shown in Fig 17(b).

Figure 15. Picture of the Cone-Ogive-Cylinder being tested in the BAM6QT.

Figure 16. Picture of the Cone-Ogive-Cylinder after being painted with Temperature Sensitive Paint.

2. Flared Design Results

Figure 18 is a picture of the flared cone designed by Lindsay Kirk to maximize the N-factors of the first mode instabilities. In the photo the 0.32 meter sharp nosetip has been removed from the 0.43 meter body. The original design had a total length of one meter, but the model design was truncated at 0.75 meters when machined because that is the estimated useful length before the reflected shocks would start impacting the instability measurements.

The flared cone was built with the goal of measuring at some location, both first and second mode instabilities. As an initial step to analyze these instabilities in the flared design, three Kulite high frequency pressure sensors were installed flush with the surface at 0.53, 0.60, and 0.68 meters downstream of the nosetip. The BAM6QT was tested over a range of quiet and noisy stagnation pressures. Second mode instabilities were measured using the transducers starting at a stagnation pressure of 120 psia. This instability showed up most clearly at 0.6 meter downstream as shown by the large bumps peaking between about 140 and 170 kHz in Fig 19. A comparison of the power spectral densities at two of the locations show the instability increasing in magnitude and decreasing slightly in frequency as it progresses downstream.

Figure 19 also shows evidence of possible first-mode instabilities as shown in the peak at around 60 kHz that occurs for stagnation pressures above 80 psia at 0.53m. However, for some reason the transducer at 0.6m does not show any instability at this frequency. Further tests will be conducted to see if first-mode instabilities can be conclusively measured on this cone. No instability frequencies were measured during any of the noisy runs. The tunnel noise seemed to be larger than any instabilities that may have been present.

V. Shock Tube Calibrations of PCB-132 Sensors

A half-scale version of the 6-inch (15.2-cm) shock tube in the Graduate Aerospace Laboratories at Caltech (GALCIT) has recently been completed at Purdue. This shock tube has a 8.9-cm inner diameter, a 3.6-m driven section, and a 0.9-m driver section. The driven section is designed to reach pressures of 1 millitorr (100 Pa), and the driver section can withstand pressures as high as 6895 kPa. Further details about the shock tube are provided in Reference 27.

The shock tube has been built to calibrate sensors, particularly PCB-132 sensors. These sensors have seen widespread use in hypersonic wind tunnels in recent years,[23,28–34] but are designed as time-of-arrival sensors, and were not originally intended for instability measurements. As a result, the response of the

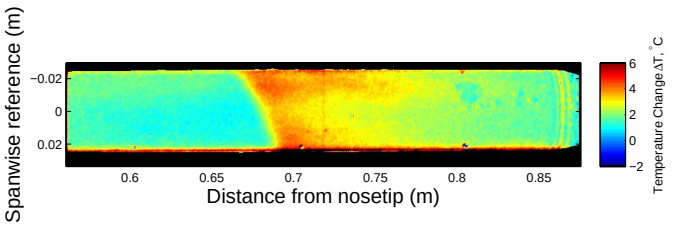

(a) TSP under Noisy flow.

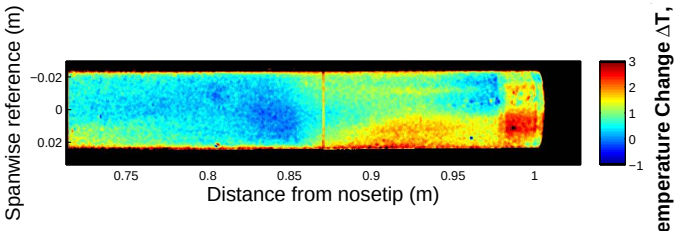

(b) TSP under Quiet Flow.

Figure 17. Temperature-Sensitive Paint showing shock locations.

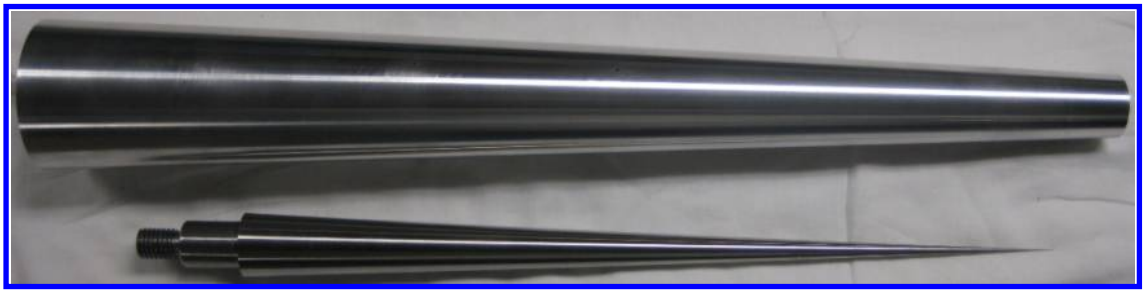

Figure 18. Picture of the Flared Cone being tested in the BAM6QT with the nosetip detached from the body.

sensors at low amplitudes, their frequency response, and their spatial resolution have not been characterized by the manufacturer. One way to determine these characteristics is to calibrate the sensors using a shock tube. The step input generated by the shock can be used to identify the response at high frequencies, and weak shocks can be created to test the response at low amplitudes. The spatial resolution can be investigated with shocks of known thickness.

Initial work towards these calibrations has been performed using the shock tube at Purdue. Characterization of the performance of the shock tube has begun, including the strength of shocks that can be created, the formation distance of these shocks, and some information regarding their planarity. Weak shocks with static pressure rises on the order of 0.1 PSI have been created, and preliminary calibration curves have been found for a small number of PCB-132 sensors. Further work will include measuring the frequency response of the sensors, measuring the spatial resolution of the sensors, and improving the quality of the low-amplitude shock waves.

VI. Initial Shock Measurements

PCB-132 sensors, Kulite XCQ-062-15A and Kulite XCE-062-50A sensors were mounted in sensor inserts, flush with the wall of the shock tube. An o-ring was used to seal around the insert, but the sensors were installed in the insert using nail polish, which provided the only seal around the sensor. Leaks were low

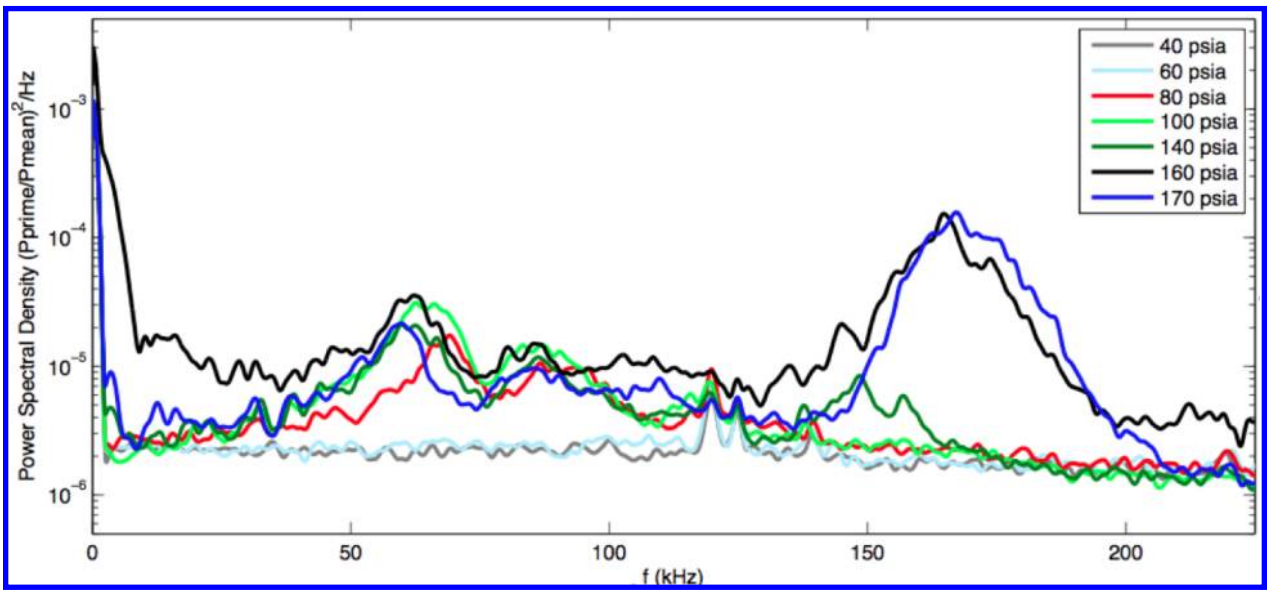

(a) PSD on Flared Design at 0.53 m.

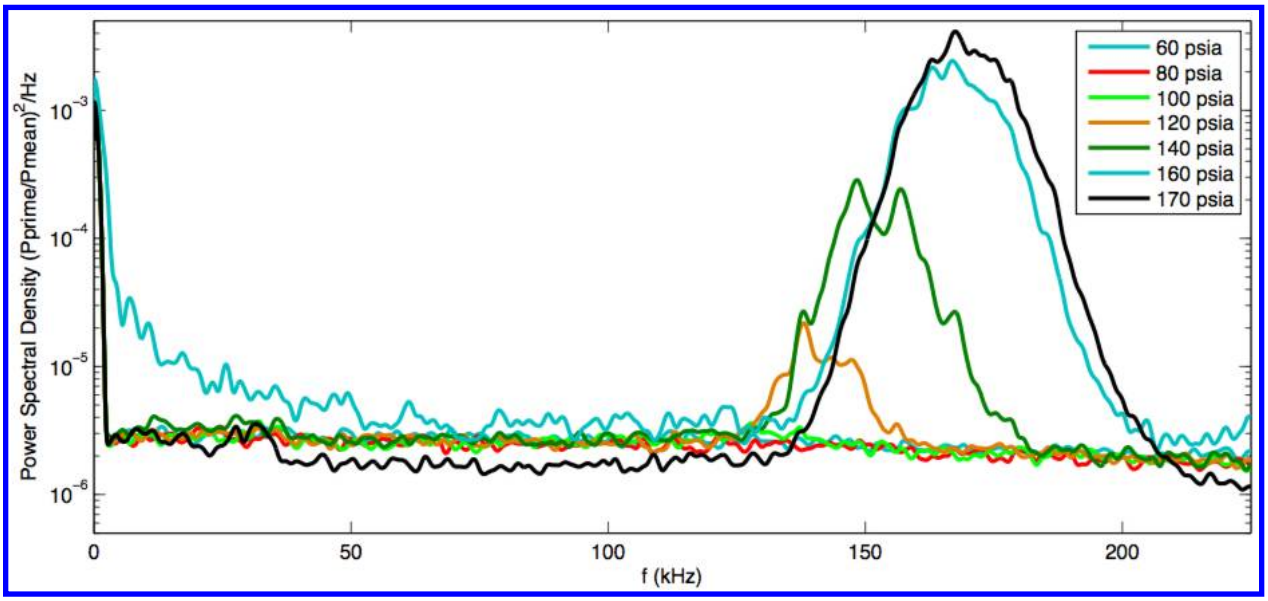

(b) PSD on Flared Design at 0.60 m.

Figure 19. PSD Results on the Flared Design over a range of Stagnation Pressures under Quiet Flow.

enough that millitorr-range pressures could be reached, but the leak rate through the nail polish was not determined.

When a shock passes, the PCB-132 shows a sharp peak, followed by a rolloff which begins almost instantly. The rolloff is caused by the 11-kHz high-pass filter inherent to the sensor. While only one shock is shown in Fig. 20, reflected shocks would simply appear as additional peaks in the trace. The height of the voltage jump is used to determine the strength of the shock. The static calibration of the Kulites is assumed to be the same as the dynamic calibration. This is an approximation, but should be close enough for reasonable initial results until a better reference sensor is found.

Figure 20 shows typical shock responses and illustrates some of the improvements realized with the new shock tube. The blue trace is from the shock tube used previously, and represents the response from the weakest shock that could be created in that tube. A high level of noise at high and low frequencies is visible. The sources of the noise have not been examined in detail, but some is likely attributable to electronic noise, and some to imperfections in the flow. The new shock tube is capable of creating much weaker shocks, as the much smaller peak indicates. In addition, the noise levels at all frequencies have been reduced. This reduction in noise level will be very useful for identifying the frequency response of the sensors.

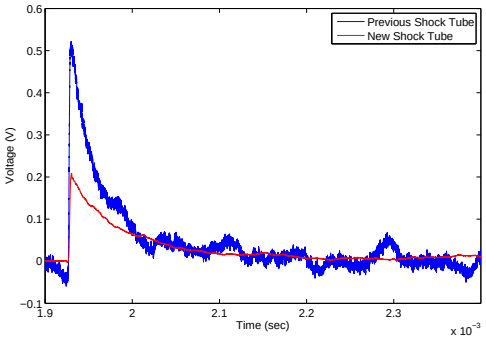

Figure 20. Shock response in the new shock tube compared to one in the previous shock tube.

The responses of the PCBs can be compared to the pressures measured by the Kulites to develop calibration curves. Some examples are shown in Fig. 21. The main concerns are whether the sensors are linear at low range, and how these calibrations compare to the manufacturer's calibrations. Linear fits with a specified offset of zero have been plotted alongside the PCB data and the manufacturer's calibration line. The curves have been plotted on both linear and logarithmic curves to better illustrate the fit at both low and high pressure steps.

The curves appear to be linear over the majority of their range, with a fairly low degree of scatter. In most cases, the calibration slope measured here is substantially lower than that found by the manufacturer. This agrees with attempts at correcting the PCB calibration slope to agree with measurements of pressure fluctuations by Kulites, which also found that the calibration slope for the PCBs needed to be reduced.[31,35] The manufacturer's calibration was found to be lower than the shock tube calibration in only one case. In the very low pressure range, less than 0.1 PSI, the linearity of the sensors becomes ambiguous. The response of the sensor is typically above the linear fit, but it is unclear if the difference is simply due to scatter, a nonlinearity, or an experimental error. Experimental error and electronic noise become significant concerns at these low amplitudes because the response of the sensors is less than 10 mV.

Work continues in the shock tube to reduce uncertainty in the weak shocks. Different reference sensors must be tried, and the planarity of the shocks must be investigated in detail. In addition, a pitot probe has been constructed which will allow measurement of the step response of the sensors. This should allow the determination of the frequency response.

VII. Conclusions

Improved methods of generating turbulent spots on the nozzle wall are under investigation. A pneumatic pulsed valve has generated large patches of turbulence, but it is unclear whether the flow generated is composed of turbulent spots or patches of quasi-steady flow. Improvements to decrease the duration of the pulses are underway. An alternative spark perturber is in the design stage, and testing will begin once the hardware arrives.

Experiments were performed with a 7° cone at 6° angle of attack, looking at the effect of discrete roughness elements on the stationary crossflow instability. The roughness elements were placed around the azimuth, near the neutral point of the most unstable stationary modes. Depending on the spacing of the roughness elements, the breakdown of the stationary vortices moved upstream, and the spacing of the vortices changed. The exact extent of the effect the roughness elements are having on the stationary vortices still needs to be determined.

Computational analyses have shown that first mode instabilities can be larger than the second mode instabilities under BAM6QT flow conditions by changing the model design. Two major design features that impact the first mode instabilities are the leading edge cone angle and the flare. The leading edge cone angle can decrease the edge Mach to the point that first mode becomes dominant. Flare has been shown to increase the magnitude of both first and second mode instabilities, but it has a greater impact on the second mode. Testing in the BAM6QT has begun to further investigate the effectiveness of the two model designs in generating first mode instabilities of a sufficient magnitude to be measured.

The 3-inch shock tube has been demonstrated to be useful for sensor calibrations. Weak shocks have been created, though additional work is needed to ensure that the shocks are of sufficiently high quality for calibrations. PCB-132 sensors appear to be linear to low amplitudes, though results close to second-mode amplitudes are ambiguous.

VIII. Acknowledgements

The authors would like to thank the Air Force Office of Scientific Research for their funding under grant number FA9550-12-1-0167. Meelan M Choudhari performed preliminary design work that helped direct us toward a feasible first-mode dominant design. Heath Johnson and Graham Candler at the University of Minnesota installed STABL on our Purdue computer and assisted in running the code. Thanks also goes to Lindsay Kirk at the University of Minnesota and Charles Campbell at NASA Johnson Space Center for Lindsay's much appreciated help in the design optimization process. Additional thanks to the Johnathan Amy Facility for Chemical Instrumentation and the Zwier group at Purdue for assistance in designing and using the pulsed valve driver.

References

[1]Schneider, S. P., "Hypersonic Laminar-Turbulent Transition on Circular Cones and Scramjet Forebodies," *Progress in Aerospace Sciences*, Vol. 40, No. 1-2, 2004, pp. 1–50.

[2]Beckwith, I. and III, C. M., "Aerothermodynamics and Transition in High-Speed WInd Tunnels at NASA Langley," *Annual Review of Fluid Mechanics*, Vol. 22, 1990, pp. 419–439.

[3]Schneider, S. P., "Flight Data for Boundary-Layer Transition at Hypersonic and Supersonic Speeds," *Journal of Spacecraft and Rockets*, Vol. 36, No. 1, 1999.

[4]Schneider, S. P., "Effects of High-Speed Tunnel Noise on Laminar-Turbulent Transition," *Journal of Spacecraft and Rockets*, Vol. 38, No. 3, May-June 2001, pp. 323–333.

[5]Johnson, C., Stainback, P., Wicker, K., and Boney, L., "Boundary-layer edge conditions and transition Reynolds number data for a flight test at Mach 20 (Reentry F)," TM X-2584, NASA, July 1972.

[6]Pate, S. and Brown, M. D., "Acoustic Measurements in Supersonic Transitional Boundary Layers," Tech. Rep. AEDC-TR-69-182, October 1969.

[7]Elder, J. W., "An experimental investigation of turbulent spots and breakdown to turbulence," *Journal of Fluid Mechanics*, Vol. 9, No. 02, October 1960, pp. 235–246.

[8]Krishnan, L. and Sandham, N., "On the merging of turbulent spots in a supersonic boundary-layer flow," *International Journal of Heat and Fluid Flow*, Vol. 27, 2006, pp. 542–550.

[9]Makita, H. and Nishizawa, A., "Characteristics of internal vortical structures in a merged turbulent spot," *Journal of Turbulence*, July 2001.

[10]Casper, K. M., *Pressure Fluctuations Beneath Instability Wave Packets and Turbulent Spots in a Hypersonic Boundary Layer*, Ph.D. thesis, Purdue University, August 2012.

[11]Casper, K., Beresh, S., and Schneider, S., "Spanwise Growth of the Turbulent Spot Pressure-Fluctuation Field in a Hypersonic Boundary Layer," AIAA Paper 2011-3873, June 2011.

[12]Senkan, S. M. and Deskin, S. C., "A continuous-purge pulsed valve suitable for high-temperature applications," *Review of Scienctific Instruments*, Vol. 68, 1997, pp. 4286.

[13]Saric, W. S., Reed, H. L., and White, E. B., "Stability and Transition of Three-Dimensional Boundary Layers," *Annual Review of Fluid Mechanics*, Vol. 35, 2003, pp. 413–440.

[14]Deyhle, H. and Bippes, H., "Disturbance Growth in an Unstable Three-Dimensional Boundary Layer and its Dependence on Environmental Conditions," *Journal of Fluid Mechanics*, Vol. 316, December 1996, pp. 73–113.

[15]Saric, W. S., Carrillo, R. B., and Reibert, M. S., "Leading-Edge Roughness as a Transition Control Mechanism," AIAA Paper 1998-0781, 1998.

[16]Corke, T., Matlis, E., Schuele, C.-Y., Wilkinson, S., Owens, L., and Balakumar, P., "Control of Stationary Cross-flow Modes Using Patterned Roughness at Mach 3.5," *7th IUTAM Symposium on Laminar-Turbulent Transition*, 2010, pp. 123–128.

[17]Schuele, C. Y., *Control of Stationary Cross-Flow Modes in a Mach 3.5 Boundary Layer Using Patterned Passive and Active Roughness*, Ph.D. thesis, University of Notre Dame, South Bend, Indiana, December 2011.

[18]Chou, A., Ward, C. A. C., Letterman, L. E., Luersen, R. P. K., Borg, M. P., and Schneider, S. P., "Transition Research with Temperature-Sensitive Paints in the Boeing/AFOSR Mach-6 Quiet Tunnel," AIAA Paper 2011-3872, June 2011.

[19]Li, F., Choudhari, M., Chang, C.-L., and White, J., "Analysis of Instabilities in Non-Axisymmetric Hypersonic Boundary Layers over Cones," AIAA Paper 2010-4643, June 2010.

[20]Radeztsky Jr., R. H., Reibert, M. S., and Saric, W. S., "Effect of Isolated Micron-Sized Roughness on Transition in Swept-Wing Flows," *AIAA Journal*, Vol. 37, No. 11, 1999, pp. 1370–1377.

[21]Ward, C. A. C., Wheaton, B. M., Chou, A., Berridge, D. C., Letterman, L. E., Luersen, R. P. K., and Schneider, S. P., "Hypersonic Boundary-Layer Transition Experiments in the Boeing/AFOSR Mach-6 Quiet Tunnel," AIAA Paper 2012-0282, January 2012.

[22]Johnson, H. B., "Stability and Transition Analysis for Hypersonic Boundary Layers Program Reference," Tech. rep., 2010.

[23]Berridge, D. C., Casper, K. M., Rufer, S. J., Alba, C. R., Lewis, D. R., Beresh, S. J., and Schneider, S. P., "Measurements and Computations of Second-Mode Instability Waves in Several Hypersonic Wind Tunnels," AIAA Paper 2010-5002, June 2010.

[24]Schneider, S. P., Personal Email, 2011.

[25]Choudhari, M. M., Email to Steven Schneider, 2011.

[26]Zucrow, M. J. and Hoffman, J. D., *Gas Dynamics, Multidimensional Flow*, Vol. 2, Robert E. Krieger Publishing Company, Malabar, Florida, 2nd ed., 1985.

[27]Berridge, D. C., Ward, C. A., Luersen, R. P., Chou, A., Abney, A. D., and Schneider, S. P., "Boundary-Layer Instability Measurements in a Mach-6 Quiet Tunnel," AIAA Paper 2012-3147, June 2012.

[28]Fujii, K., "Experiment of Two Dimensional Roughness Effect on Hypersonic Boundary-Layer Transition," *Journal of Spacecraft and Rockets*, Vol. 43, No. 4, July-August 2006, pp. 731–738.

[29]Estorf, M., Radespiel, R., Schneider, S. P., Johnson, H., and Hein, S., "Surface-Pressure Measurements of Second-Mode Instability in Quiet Hypersonic Flow," AIAA Paper 2008-1153, January 2008.

[30]Alba, C., Casper, K., Beresh, S., and Schneider, S., "Comparison of Experimentally Measured and Computed Second-Mode Disturbances in Hypersonic Boundary-Layers," AIAA Paper 2010-897, January 2010.

[31]Bounitch, A. and Lewis, D. R., "Improved Measurements of "Tunnel Noise" Pressure Fluctuations in the AEDC Hypervelocity Wind Tunnel No. 9," AIAA Paper 2011-1200, January 2011.

[32]Tanno, H., Komuro, T., Sato, K., Itoh, K., Takahashi, M., and Fujii, K., "Measurement of Hypersonic Boundary Layer Transition on Cone Models in the Free-Piston Shock Tunnel HIEST," AIAA Paper 2009-0781, January 2009.

[33]Bountin, D., Chimitov, T., Maslov, A., Novikov, A., Egorov, I., and Fedorov, A., "Stabilization of a Hypersonic Boundary Layer Using a Wavy Surface," AIAA Paper 2012-1105, January 2012.

[34]Munoz, F., Heitmann, D., and Radespiel, R., "Instability Modes in Boundary Layers of an Inclined Cone at Mach 6," AIAA Paper 2012-2823, June 2012.

[35]Beresh, S. J., Henfling, J. F., Spillers, R. W., and Pruett, B. O., "Measurement of Fluctuating Wall Pressures Beneath a Supersonic Turbulent Boundary Layer," AIAA Paper 2010-305, January 2010.

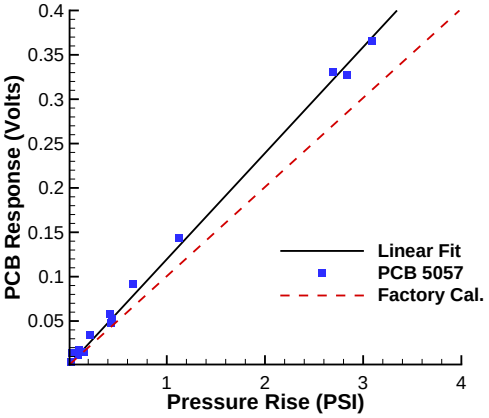

(a) #5057, Linear scale

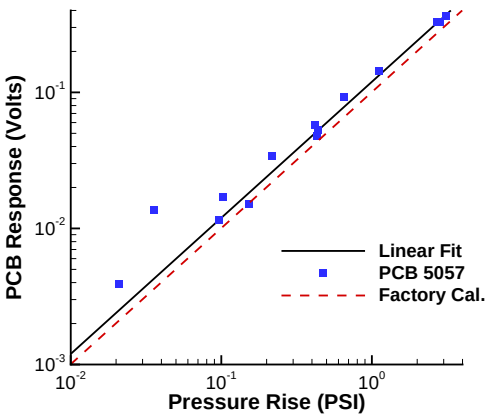

(b) #5057, Logarithmic scale

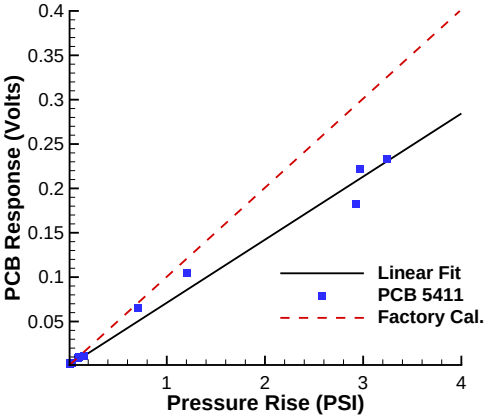

(c) #5411, Linear scale

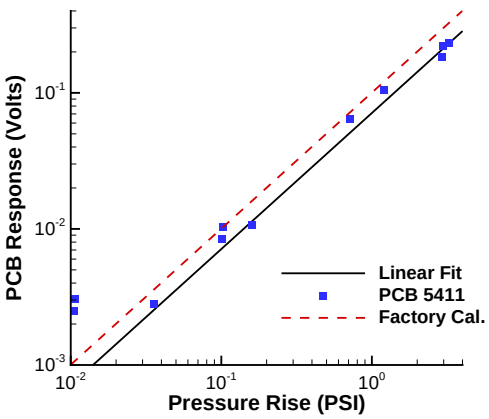

(d) #5411, Logarithmic scale

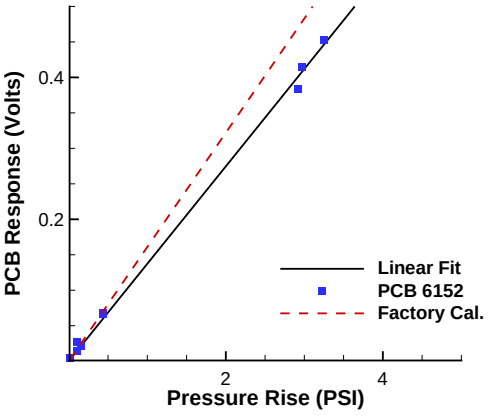

(e) #6152, Linear scale

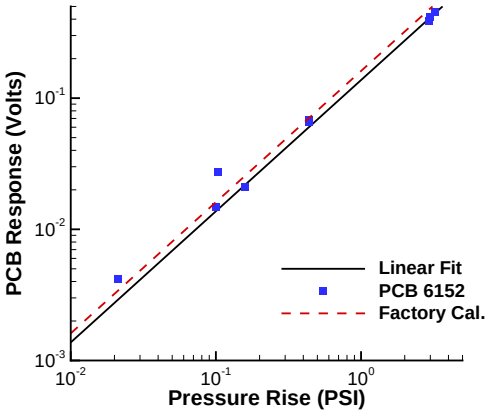

(f) #6152, Logarithmic scale

Figure 21. Initial Calibration Curves for PCB-132 Sensors